©Freund Publishing House Ltd. International Journal of Nonlinear Sciences and Numerical Simulation 6(3),235-242, 2005

Equivalency and Locality in Nano-scale Measurement

Ming Hu[1, 2]

1. *State Key Laboratory of Nonlinear Mechanics (LNM), Institute of Mechanics, Chinese Academy of Sciences, Beijing 100080, China*
2. *Graduate School of Chinese Academy of Sciences, Beijing 100039, China*

Email: huming@lnm.imech.ac.cn

Haiying Wang, Yilong Bai

LNM, Institute of Mechanics, Chinese Academy of Sciences, Beijing 100080, China

Mengfen Xia

Department of Physics, Peking University, Beijing 100871, China

Fujiu Ke

Department of Applied Physics, Beijing University of Aerospace and Aeronautics, Beijing 100083, China

Communicated by Ya-Pu Zhao

Abstract

Two principal problems of equivalency and locality in nano-scale measurement are considered in this paper. The conventional measurements of force and displacement are always closely related to the equivalency problem between the measuremental results by experimental system and the real physical status of the sample, and the locality of the mechanical quantities to be measured. There are some noticeable contradictions in nano-scale measurements induced by the two problems. In this paper, by utilizing a coupled molecular-continuum method, we illustrate the important effects of the two principal problems in atomic force microscopy (AFM) measurements on nano-scale. Our calculations and analysis of these typical mechanical measurement problems suggest that in nano-meter scale measurements, the two principal problems must be carefully dealt with. The coupled molecular-continuum method used in this paper is very effective in solving these problems on nano-scale.

Keywords: nano-meter scale measurement, nonlocality effect, equivalency, atomic force microscopy, van der Waals forces, coupled molecular-continuum method

1. Introduction

The rapid development of the micro/nano-electro-mechanical systems (MEMS /NEMS) and some related technologies has led the science of mechanics to focus increasingly on the nano-scale [1-7]. This is a new challenge and opportunity in the 21st century. Obviously, proper nano-meter scale mechanical measurement is one of the prerequisites to the further and solid development of MEMS/NEMS.

In conventional measurements of force and displacement, it's always expected that the output signals of measurement system are the exact force acting on the sample and the deformation of the sample. Actually, this should be closely related to the equivalency problem between the experimental system and the sample, and the locality of the mechanical responses of the sample. These two problems can result in some noticeable contradictions in nano-meter scale measurements. So, in the nano-meter scale measurements, we must consider these two problems carefully. In this paper, a coupled molecular-continuum method is used to illustrate the important effects of the two principal problems in the measurements on nano-meter scale.

For example, atomic force microscopy is one of the instruments commonly used for nano-meter scale measurements. In 1986, Binnig and Rohrer were rewarded with the Nobel Prize in Physics for their eximious invention of STM,

which provided a breakthrough in our ability to investigate matter on atomic scale. In the same year, Binnig et al [8] invented the Atomic Force Microscopy. In fact, a number of experiments have been done so far on a variety of layered materials such as graphite [9, 10] and boron nitride (BN) [10], ionic crystals such as NaCl [11], and even biological substrates like DNA fragments [12].

It is well known, in AFM measurement, there are various atomic and molecular forces between the tip of instrument and the sample, e.g. van der Waals forces. The force acting on the tip is detected by a micro-cantilever according to its deformation. At the same time, the instrument adjusts the position of the sample and the fixed end of the cantilever to keep the force unchanged [13]. The adjustment is taken to interpret the surface morphology of the sample. Therefore, the cantilever is used not only as the loading part but also as the sensing part of the measurement system. In order to make the response of a sample equivalent to that of the experimental system, it's required that the stiffness of the loading system, namely the cantilever, should be as high as possible and the stiffness of the sensing system (the cantilever) is as low as possible. Obviously, the equivalency principle is hard to be satisfied completely in an AFM system.

On the other hand, the locality assumption means that the load acting on the tip exactly results from the point, on the sample, right opposite the tip apex, regardless of the vicinity of the point. However, in the nano meter scale measurements, the AFM tip is of nano-meter magnitude, and in most cases, asperities on a sample surface are of the same order as the tip radius. When we use AFM to detect the surface morphology of a sample, the interaction between the tip and the sample is not only related to the local area of their opposite position, but also related to the status nearby. This may lead to some un-negligible deviation. Then, the locality assumption needs careful re-examining. That is to say, one should ask whether the output given by an AFM is the real surface morphology of a sample.

In the present work, by utilizing a coupled molecular-continuum method, which avoids the formidable difficulty in computing ability ant time scales in molecular dynamics (MD) simulation [14], we detailedly investigated the important effects of the two principal problems in atomic force microscopy measurements on nano-meter scale. Our paper is organized as follows. First, we briefly introduced the working principle of AFM. Then in section 3, we described our calculation model and method. In section 4, we studied the equivalency problem in AFM force-distance curve measurements. We compared the real tip-sample force-distance curve with the measured one based on our calculation results and found that they are not exactly superposed. Furthermore we explained the jump-in and jump-off phenomena appearing in the recording when the tip approaches the sample surface and separates away. In section 5, we used the coupled method to investigate the nonlocality problem involved in AFM measurement of the morphology of rough surface. Finally, we give our conclusion in section 6.

2. Working Principle of AFM

Figure 1 shows the classical AFM instrument.

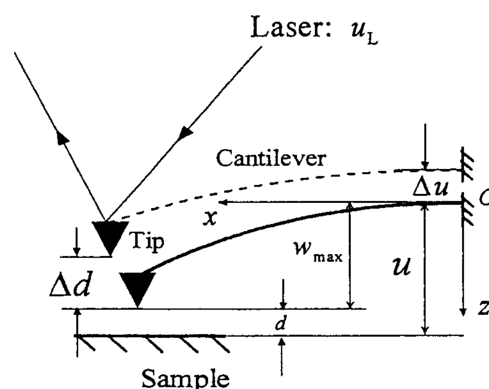

Fig. 1 Schematic of AFM measurement instrument

In Fig. 1, d is distance between the tip and the sample surface, and u is the position of fixed end of the cantilever. Both of them are two basic measuremental quantities in AFM experiments. This measuremental system can be simplified as a cone-shaped tip interacting with a hemi-infinite body (see Fig. 2). From elementary geometry we know that

$$d = u - w_{max}, \tag{1}$$

where w_{max} is the deformation of the free end of the cantilever. After measuring u and w_{max}, from Eq. (1), we can deduce the tip-sample distance d. At the same time, the force signal F output by AFM can be deduced from the deformation of the cantilever.

For the typical rectangular Si_3N_4 cantilever, the length $l = 100\mu m$, the width $b = 10\mu m$ and the thickness $h = 0.6\mu m$, the mass density $\rho_{Si_3N_4} = 3.1\times10^3 kg/m^3$ [13]. So, the weight of the cantilever is $1.86\times10^{-11}N$, and the weight of the conical-like silicon tip, which is attached to the free end of the cantilever, can be estimated as $\frac{1}{3}\pi R_t^2 D_{max}\rho_{Si}g$, i.e., $\frac{\pi}{3}\times\left(10\times10^{-6}\right)^3\times2.33\times10^3\times10N=2.4\times10^{-11}N$. We see that these two weights are of the same order $O\left(10^{-11}N\right)$, but they are at least 2 magnitude smaller than the typical quantity ($10^{-9}N$, [15, 16]). Hence, the linear superposition principle is applicable to the cantilever. In our calculation, we take the deformed position of the cantilever due to the gravity as the zero point of d and w_{max}.

Neglecting all dampness and assuming all the tip-sample forces are acting on the free end of the cantilever, according to the classical elastic theory, we can obtain the force

$$F = k\cdot w_{max} = \frac{3EI}{l^3}w_{max}, \tag{2}$$

where k is the elastic constant (stiffness coefficient), E and I are the elastic modulus and inertia moment respectively, $I = \frac{1}{12}bh^3$.

3. Calculation Model and Method

In our calculation, we analyze the micro-cantilever by conventional continuum mechanics, but for the tip and the local area of the sample, we take the intermolecular interaction between them into account. This is called coupled molecular-continuum method.

As shown in Fig. 2, the tip is considered to be made up of a truncated cone and a spherical cap.

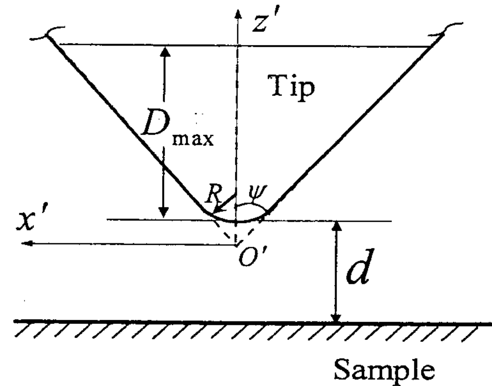

Fig. 2 Tip-sample interaction model

D_{max} is the truncated height of the whole tip, R is the curvature radius of the tip apex and ψ is the half apex angle. The sample is considered as a half-infinite body.

In our calculation, we consider the intermolecular potential function between the tip and sample as the well-known L-J 6-12 pair potential

$$e(r) = \frac{Cr_0^6}{r^{12}} - \frac{C}{r^6}, \tag{3}$$

where the first term of right hand side is related to the repulsive potential and the second term attractive potential. C is the constant representing the interaction potential and the parameter r_0 can be considered as a characteristic length in intermolecular interaction, typically taken as $0.3nm$.

The interaction potential energy between the tip and sample W_{ts}^{tot} is composed of 4 parts

$$W_{ts}^{tot} = W_{tc,s}^{rep} - W_{tc,s}^{att} + W_{sc,s}^{rep} - W_{sc,s}^{att}, \tag{4}$$

where the subscripts 't', 's', 'tc' and 'sc' represent the tip, the sample, the truncated cone and the spherical cap respectively, and the superscripts 'rep' and 'att' represent the repulsive and attractive potential energy respectively. In Fig. 2, we set up local orthogonal coordinates $O'x'z'$ at the tip apex. From Eq. (4), the z' component of the interaction force between the tip and the sample can be expressed by

$$f^{z'} = -\frac{\partial W_{ts}^{tot}}{\partial d}. \tag{5}$$

As we are basically interested in the z' component in this study, the z' component is denoted by f for simplicity in the following part of this paper.

With the assumption of additivity, the attractive interaction energy between the truncated cone and the hemi-infinite plane surface will be the sum of its interactions with all the molecules in the pair [17]. Therefore

$$W_{\text{tc,s}}^{\text{att}} = \frac{Atg^2\psi}{6}\int_{R_2}^{R_1}\frac{z'^2}{[z'+d-(R/\sin\psi - R)]^3}dz' \quad (6)$$

where

$R_1 = D_{\max} + R/\sin\psi - R$, $R_2 = R/\sin\psi - R\sin\psi$, $A \equiv \pi^2 C\rho_1\rho_2$ is the Hamaker constant, ρ_1 and ρ_2 is the number density of molecules in the tip and the sample respectively. Similarly we can calculate the other parts of $W_{\text{ts}}^{\text{tot}}$:

$$W_{\text{tc,s}}^{\text{rep}} = \frac{Ar_0^6 tg^2\psi}{45}\int_{R_2}^{R_1}\frac{z'^2}{\left[z'+d-(R/\sin\psi - R)\right]^9}dz' , \quad (7)$$

$$W_{\text{sc,s}}^{\text{att}} = \frac{A}{6}\int_{R_3}^{R_2}\frac{[z'-(R/\sin\psi - R)](R+R/\sin\psi - z')}{[d+z'-(R/\sin\psi - R)]^3}dz' \quad (8)$$

and

$$W_{\text{sc,s}}^{\text{att}} = \frac{Ar_0^6}{45}\int_{R_3}^{R_2}\frac{[z'-(R/\sin\psi - R)](R+R/\sin\psi - z')}{[d+z'-(R/\sin\psi - R)]^9}dz' , \quad (9)$$

where $R_3 = R/\sin\psi - R$. Substituting Eqs. (6)-(9) into Eqs. (4) and (5), we can obtain the expressions of $W_{\text{ts}}^{\text{tot}}$ and f.

4. Analysis of Equivalency Principle in AFM Measurements

4.1. Non-equivalency between the real force-distance curve and the measured one

In this section, we investigate the equivalency between the output $F \sim u$ curve by AFM instruments and the real force-distance curve $f \sim d$, where F and f is the output force signal by AFM and the real interaction force between the AFM tip and the sample.

We take the same parameters as those used before in estimating the weight of the cantilever and the tip. For elastic modulus of the cantilever, we take $E = 300\text{GPa}$ [13]. The parameters for silicon tip are: $R = 10\text{nm}$, $D_{\max} = 1\mu\text{m}$ and $\psi = 65^\circ$. So, the Hamaker constant for silicon tip and sample is $1.865\times10^{-19}\text{J}$ [18, 19]. From Eqs. (5)-(9), we can obtain the real tip-sample force-distance curve $f \sim d$, as shown in Fig. 3. Simultaneously, according to Eqs. (1) and (2) and the calculated $f \sim d$ curve, we can deduce the 'measured' force-distance curve $F \sim u$, as illustrated in Fig. 4.

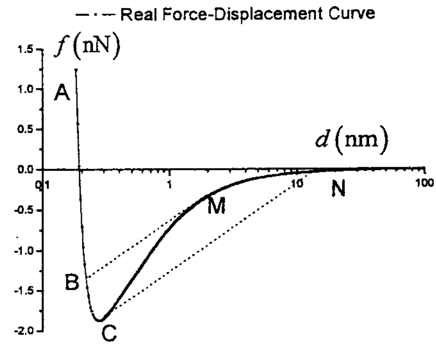

Fig. 3 Real force-displacement curve

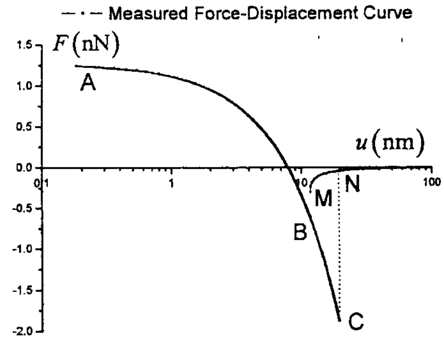

Fig.4 Measured force-displacement curve

The solid line in Fig. 3 is the real tip-sample force-distance curve $f \sim d$, which represents the real physical interaction between the tip and the sample. Figure 4 (The abscissa values in Fig. 4 have been shifted by +7.7nm to compare with Fig. 3) gives the measured force-distance curve $F \sim u$, which can be directly output by AFM instruments. The $F \sim u$ curve represents the coupling response of the whole experimental system made up of the tip, cantilever and the sample, i.e., the superposition of the mechanical response of the cantilever and the tip-sample interaction. The curves NM, BA and ACN in Fig.

3 are completely corresponding to those in Fig. 4. Therefore, it's quite reliable to deduce the real tip-sample interaction from the measuremental information given by the instrument. However, there exists one part of the real force-distance curve that can not be deduced by this way. For example, the MC part in Fig. 3. Actually, MC is corresponding to MB (the dotted line in Fig. 4) when the tip is approaching the sample surface, but is to CN when the tip-sample separates away. It's worthwhile to note that, in the MB and CN part of the measured force-distance curve, the force is not the monodrome function of the distance. So the system state shift from M to B or from C to N is an unstable process.

4.2. Stability analyses of AFM measuremental system

In this section, we detailedly explain the reason that the MC part in the measured force-distance curve can not reflect the corresponding part in the real one.

For the whole system composed of the cantilever, tip and sample, the total energy U^{tot} can be expressed as

$$U^{tot} = U^{c} + K^{c} + K^{t} + W_{ts}^{tot}, \qquad (10)$$

where U^{c} and K^{c} is Hooke's elastic potential energy and kinetic energy of the cantilever respectively, K^{t} is the kinetic energy of the tip, and W_{ts}^{tot} is the interaction energy between the tip and the sample, as denoted in Sec. 3. For the present derivation, the cantilever deformation is described by the Hooke's law

$$U^{c} = \frac{1}{2} k w_{max}^{2}, \qquad (11)$$

and as we are only interested in the quasi-static experimental process in this section, we assume

$$K^{c} = K^{t} = 0. \qquad (12)$$

For the system to be in stable equilibrium, we must have

$$\frac{\partial U^{tot}}{\partial d} = 0 \qquad (13)$$

and

$$\frac{\partial^2 U^{tot}}{\partial d^2} > 0. \qquad (14)$$

Equation (13) is the condition for U^{tot} to be stationary, and Eq. (14) gives the stability condition for the system, i.e.

$$\frac{\partial f}{\partial d} < k. \qquad (15)$$

Accordingly, the critical condition is

$$\frac{\partial f}{\partial d} = k. \qquad (16)$$

It is indicated that, if the force gradient is larger than the elastic constant, the cantilever becomes unstable and "jumps" onto or off the sample surface. This is the jump-to-contact or jump-off-contact discontinuity as shown in Fig. 4 (dotted line). From Eq. (16) the cantilever position u_M or u_C at which the jump-to-contact or jump-off-contact occurs can be determined. That is to say, in MC part of the real force-distance curve in Fig. 3, the system is unstable (tip jumping), therefore it is understandable that the measured curve fails to reflect this part in AFM measurements. In the final analysis, this is induced by the special working principle of AFM instruments. On one hand, in order to avoid these unstable phenomena, it is required that the elastic constant of the cantilever should be as high as possible. On the other hand, for the sake of high force resolution, it is expected that the elastic constant should be as low as possible. Apparently the two sides are incompatible. In practical experiments, we should make a trade-off between them. This problem is ineluctable in AFM measurements as long as the working principle doesn't change.

5. Analysis of the Nonlocality Effect in AFM Surface Morphology Measurements

In this section, we investigate another important problem in AFM measurements.

Usually there are some nano-scale structures, such as artificially designed structures in nano-devices as well as the ineluctable disordered roughness on the surface of samples. It is well known that finite tip has limitation to detect the morphology with deep valley [13]. However, it is rare known that owing to the nonlocality effect even an individual atom tip can not give exact morphology by means of the assumption of locality. Here we study a simple case to reveal this nonlocality problem in AFM surface

morphology measurements.

5.1. Calculation Model

In this investigation of the nonlocality, we assume the AFM tip to be a small sphere to scan a specified rough surface, as shown in Fig. 5.

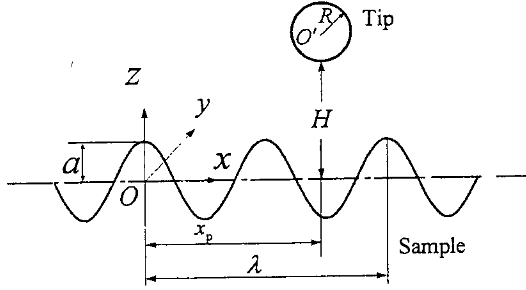

Fig. 5 Schematic diagram of an AFM tip scanning a specified rough surface

The sample surface is composed of an ideal plane surface with cosine like asperities periodically collocated with amplitude a and wavelength λ. The sample is hemi-infinite in z direction and infinite in x and y direction, and then the sample surface function is

$$z_s = a\cos\left(\frac{2\pi}{\lambda}x\right), \tag{17}$$

as shown in Fig. 5. For simplicity and convenience, the tip is replaced by a sphere with radius R. The separation between the tip and surface is denoted by H, and x_p is the tip position in the horizontal direction.

The interaction potential energy between the tip and the rough sample $W_{t,rs}^{tot}$ can be written as

$$W_{t,rs}^{tot} = W_{tf}^{rep} - W_{tf}^{att} + W_{ta}^{rep} - W_{ta}^{att}, \tag{18}$$

where the subscripts 'rs', 'f' and 'a' represent the rough sample, the hemi-infinite body and the asperities respectively, and the other scripts are the same as those in Sec. 3. The vertical component of the interaction force can be expressed by

$$f_{t,rs} = -\frac{\partial W_{t,rs}^{tot}}{\partial H}. \tag{19}$$

By the same way we did in Sec. 3, we can calculate the $f_{t,rs}$ for the respective values of H and x_p, i.e. the specified tip position.

We performed the force calculations by choosing a z interval, in which the root of the equation

$$f_{t,rs} = f_{fixed} \tag{20}$$

lies for a fixed x_p, where f_{fixed} is the prefixed scanning force. Through the golden search method [20], we can "solve" Eq. (20) within relative error 1% to f_{fixed}. When this procedure is repeated for several x_p values in one period, that is to say, $0 \le x_p \le \lambda$, the AFM image with a constant scanning force of f_{fixed} can be obtained.

5.2. Results of Single-atom Tip

To reveal the intrinsic reason that induces the nonlocality effect, we use the model of a single-atom tip which represents the virtual sharpest tip. Specifically we investigate this single-atom tip model in a number of cases with both amplitude a and the wavelength λ of asperities varying from $10r_0$ to $300r_0$. By assuming the tip be diamond and the sample be silicon, we can take the Hamaker constant $A \equiv \pi^2 C\rho_1\rho_2 = 1.13\times10^{-19}\,\mathrm{J}$ in our calculation, provided $A = 1.13\times10^{-19}\,\mathrm{J}$ (corresponding to $C = 1.27\times10^{-77}\,\mathrm{Jm}^6$) [18, 21]. All the following quantities with length dimension are divided by r_0, and those with force dimension are divided by C/r_0^7.

According to the essential AFM working principle, when fixing the scanning force f_{fixed} in Eq. (20), for every tip position x_p, we can deduce the corresponding separation $H(x_p)$ which represents the "measured" surface morphology of the sample. Now let the particle be so close to the sample surface that the AFM can work in contact mode. With the assumption of $f_{fixed} = 1.953$ (0.1nN), we can obtain the "measured" morphology scanned by the single-atom tip, as shown in Fig. 6. For comparing, we also draw the real surface morphology of the sample in Fig. 6.

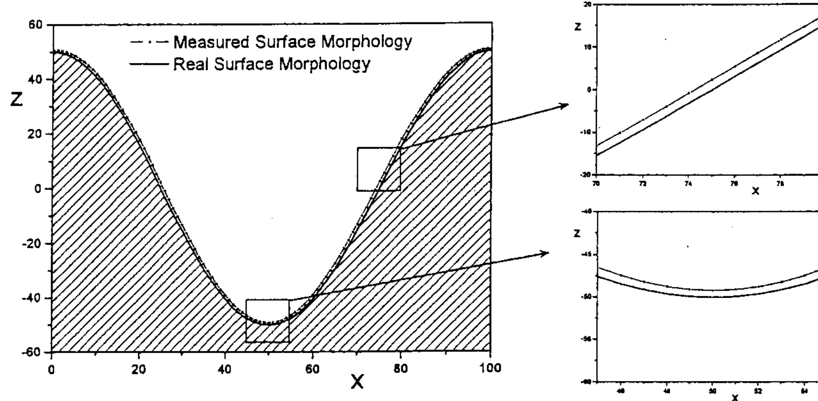

Fig. 6 Comparison of the real (real line) and measured (dashdotted line) surface morphology scanned by a single particle in one asperity period with $a = 50$, $\lambda = 100$ and $f_{\text{fixed}} = 1.953$.

From Fig. 6, we can see that in the case of the single-atom tip, the measured and real surface morphology are almost identical, except the slight difference (see the two insets in Fig. 6). In order to characterize the discrepancies between the measured and real surface morphology, we define a parameter

$$S_{\text{d}} \equiv \sqrt{\sum_{i=1}^{N_{\text{p}}} (z_{\text{m}} - z_{\text{r}})^2} \Big/ \sqrt{\sum_{i=1}^{N_{\text{p}}} z_{\text{r}}^2}, \quad (21)$$

where N_{p} is the number of calculating points in one asperity period, z_{m} and z_{r} are the measured and real surface positions respectively. For $a = 50$, $\lambda = 100$ and $f_{\text{fixed}} = 1.953$ in Fig. 6, $S_{\text{d}} = 1.59\%$. This suggests that the nonlocality effect in AFM measurement with a single-atom tip is not very strong when $a \gg 1$ and $\lambda \gg 1$, and the measured results are believable.

However, for deep (with increasing a) and closer (decreasing λ especially close to characteristic length scale r_0) asperities, the parameter S_{d}, namely the indicator of the nonlocality effect of the measured results, will increase sharply. Figures 7(a) and 7(b) show the curves of S_{d} varying with wavelength λ and amplitude a respectively.

These figures indicate that S_{d} increases with increasing a or decreasing λ, that is to say, the more rough the sample surface is, the more pronounced the nonlocality effect of measured morphology is.

From Figs. 7(a) and 7(b), we can approximately draw out the influence zone in the a - λ space, as illustrated in Fig. 8.

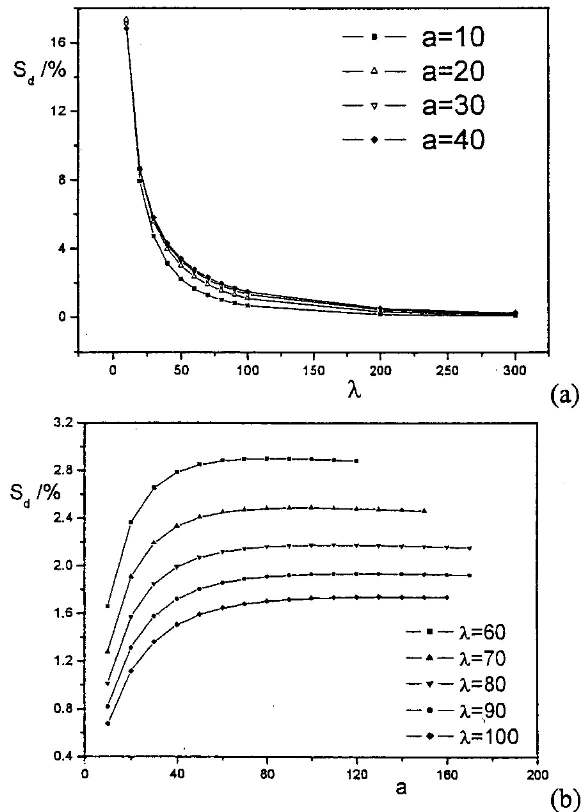

Fig. 7 (a) S_{d} vs λ curves for various a changing from 10 to 40; (b) S_{d} vs a curves with λ varying from 60 to 100. Both figures are calculated under constant scanning force 0.1nN.

Now, it can be concluded that the nonlocality effect of the measured morphology may be significant when a - λ parameter lies in zone I, while inconspicuous in zone II (at least $\lambda > 10$). From the model of single-atom tip, where there is a characteristic intermolecular interaction distance r_0, we can conclude that the nonlocality effect on morphology measurement made by AFM under constant load mode is intrinsic, regardless of the finite size of AFM tip.

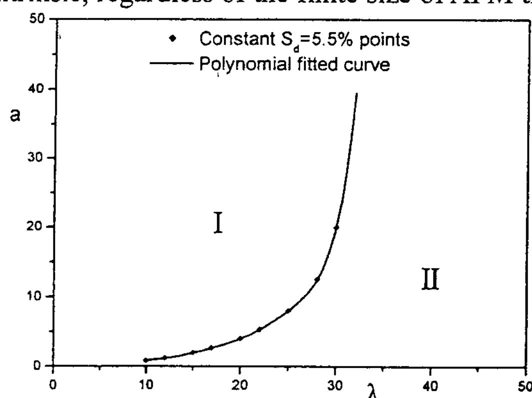

Fig. 8 Constant $S_d = 5.5\%$ curve fitted by polynomial. The points are calculated under constant scanning force 0.1nN.

6. Summary

In summary, by using a coupled molecular-continuum method, we have analyzed two important problems (equivalency and nonlocality) in AFM measurements. It is found that the non-equivalency problem is ineluctable and the nonlocality problem is intrinsic. In particular, the effects of non-equivalency and nonlocality may become significant for high and dense asperities. The calculations and analysis of these two typical mechanical measurement problems suggest that in nano-meter scale measurements, one must deal with the above two principle problems carefully. The coupled molecular-continuum method used in this paper is very effective in solving these problems on nano-meter scale.

Acknowledgements

This work is financially supported by the Chinese Academy of Sciences (KJCX2-SW-L2) and the National Natural Science Foundation of China (10432050) and the Major State Research Project of China (G2000077305)

References

1. Wei, Z., Zhao, Y.P. *Chinese Physics Letters*, **21**(4) (2004) 616-619
2. Li, D.C., Xiao, Z.Y., Wu, et al. *Int. J. Nonl. Sci.& Num. Simulation*, **3**(3-4) (2002) 341-344
3. Gong, F.F., Sun, Q.P. *Int. J. Nonl. Sci.& Num.Simulation*,**3**(3-4) (2002) 379-382
4. Wang, H.Y., Bai, Y.L. *Int. J. Nonl. Sci.& Num.Simulation*,, **3**(3-4) (2002) 433-436
5. Sun, K.H., Qian, J., Zhang, L.X., et al. *Journal of Mechanical Strength*, **23**(4) (2001) 488-494
6. Lin, J.S., Ju, S.P. *Int. J. Nonl. Sci. & Num.Simulation*,**3**(3-4) (2002) 707-711
7. Ren, S.L., Yang, S.R., Zhao, Y.P., et al. *Int. J. Nonl. Sci.& Num .Simulation*, **3**(3-4) (2002) 785-788
8. Binnig, G. *Physical Review Letters*, **56**(9) (1986) 930-933
9. Mati, O., Drake, B., Hansma, P.K. *Applied Physics Letters*, **51**(7) (1987) 484-486
10. Albrecht, T.R., Quate, C.F. *Journal of Applied Physics*, **62**(7) (1987) 2599-2602
11. Meyer, M., Amer, N.M. *Applied Physics Letters*, **56**(2) (1990) 2100-2101
12. Thundat, T., Warmack, R.J., et al. *J. Vacuum Sci. & Technology A*, **10**(4) (1992) 630-635
13. Bai, C.L. *Technique of scanning force microscope* (in Chinese), Science Press, Beijing, 2000
14. Kadau, K., Germann, T.C., et al. *PNAS*, **101**(16) (2004) 5851-5855
15. Thundat, T., Zheng, X.Y., Chen, G.Y. *Applied Physics Letters*, **63**(15) (1993) 2150-2152
16. Xu, L., Lio, A., Hu, J. *Journal of Physical Chemistry B*, **102**(3) (1998) 540-548
17. Israelachvili, J.N. *Intermolecular and surface forces*, Academic Press, London, 1985
18. Senden, T.J., Drummond, C.J. *Colloids and Surfaces A*, **94** (1995) 29-51
19. French, R.H., Canon, R.M., DeNoyer, L.K. *Solid State Ionics*, **75** (1995) 13-33
20. Press, W.H., Teukolsky, S.A., Vetterling, W.T., Flannery, B.P. *Numerical recipes in Fortran 77: the art of scientific computing (Vol. 1 of Fortran numerical recipes)*, Cambridge University Press, Cambridge, 1992
21. Fernandez-Varea, J.M., Garcia-Molina, R. *J. Colloid and Interface Science*, **231**(2) (2000) 394-397